Strong Gravitational Lensing and Catastrophe Theory

Soniya Sharma

A dissertation submitted for the partial fulfilment of BS-MS dual degree in Science

Indian Institute of Science Education and Research, Mohali

April 2014

Certificate of Examination

This is to certify that the dissertation titled **Strong Gravitational Lensing and Catastrophe Theory** submitted by **Soniya Sharma** (Reg. No. MS09124) for the partial fulfillment of BS-MS dual degree programme of the Institute, has been examined by the thesis committee duly appointed by the Institute. The committee finds the work done by the candidate satisfactory and recommends that the report be accepted.

Dr. H.K Jassal   Dr. Sudeshna Sinha   Dr. Jasjeet Singh Bagla
                                                                    (Supervisor)

Dated: April 25, 2014

Declaration

The work presented in this dissertation has been carried out by me under the guidance of Dr.Jasjeet Singh Bagla at the Indian Institute of Science Education and Research Mohali.

This work has not been submitted in part or in full for a degree, a diploma, or a fellowship to any other university or institute. Whenever contributions of others are involved, every effort is made to indicate this clearly, with due acknowledgement of collaborative research and discussions. This thesis is a bonafide record of original work done by me and all sources listed within have been detailed in the bibliography.

Soniya Sharma
(Candidate)

Dated: April 25, 2014

In my capacity as the supervisor of the candidate's project work, I certify that the above statements by the candidate are true to the best of my knowledge.

Dr. Jasjeet Singh Bagla
(Supervisor)

Acknowledgment

I would like to gratefully acknowledge the support and guidance of my supervisor, Dr. Jasjeet Singh Bagla. I heartily value his advice, expert guidance, valuable suggestions, discussions and constant encouragement imparted during the course of this work and preparation of the thesis. I am also grateful to my Masters thesis committee members Dr. H. K Jassal and Dr. Sudeshna Sinha for their valuable suggestions and comments during the committee meeting.

On a personal note, I would like to thank my family for their support, both financial and moral, which has been without limits throughout my life. Finally, I would like to thank my friends for their persistent encouragement and support.

List of Figures

LIST OF FIGURES

Contents

Abstract

Gravitational lensing, bending of light rays due to gravitational potential, can lead to formation of highly distorted and multiple images of distant objects. Though the theoretical understanding of the phenomena came from predictions of Einstein's General theory of Relativity, it is since thirty years ago that it has been possible to observe it with the aid of a number of highly sensitive telescopes. Subsequently, it was understood that gravitational lensing can be used as a tool to map the gravitational potential of clusters and galaxies in detail. In the last three decades the focus has firmly been on generic and stable image configurations (cusps and folds) or on statistical determination in the limit of weak distortions. However, with improvement in sensitivity and sky coverage, rare image configurations are likely to be detected with upcoming instruments like LSST(Large Synoptic Survey Telescope). In this project we intend to identify and map different types of singularities in image plane for a given lens potential. We have also studied generic image forms for each type of singularity.

Chapter 1

Strong Gravitational Lensing

Gravitational lensing is a phenomena in which light rays are deflected by gravity. Though in the framework of Newtonian relativity, this deflection is possible, the actual value of the shift can be calculated correctly only using Einstein's General Theory of Relativity (GTR). Prediction of GTR was that a light ray which passes close to the limb of the sun would be deflected by $1.7''$. Arthur Stanley Eddington estimated such a shift observationally during a solar eclipse in 1919[3]. His measurement showed that GTR is a more favored theory for gravity over the Newtonian framework. He [3] also noted the possibility of formation of multiple images as a result of this phenomena. Einstein [4] formulated the mathematical theory of lensing due to the potential of massive stars, however, believed that owing to the limited resolution of the telescopes, there is not much hope of observing it directly. Zwicky [5] realized the possibility of the detection of gravitational lensing by the potential of the galaxies (called nebulae at that time). He calculated the probability of this detection and found that it is on the order of one percent for a source at a reasonably high redshift. It took almost half a century to detect the first gravitational lens QSO 0957+561 A, B using radio spectroscopy in 1979 [6].

Once observation of the gravitation lenses became possible, focus shifted on using it as a tool. The very important application of Gravitational Lensing is the magnification effect which enables these lenses to act as cosmic telescopes ([5]). This helps in inferring source properties which are below the detection limit of current observations. This phenomena has also led to accurate determination of mass of galaxies which act as lenses. Light from different images of the same source travel different paths and hence the time delay between them can be used to give an accurate dis-

1

tance to the lensed object provided that the lens geometry is known. Time delay can further be used for determination of cosmological parameters like the Hubble's constant. Since Gravitational Lensing depends only on the projected two dimensional mass distribution of the lens it offers an ideal way to detect and quantify the amount of dark matter.

The critical curves and caustics produced as a result of lensing has been used as a key to represent the distribution of the gravitating mass of the gravitational lenses. In principle by observing the higher order caustics formed in the image of distant quasars lensed by a foreground galaxy cluster it is possible to infer the cluster potential very accurately. This is because not many instances of higher order caustics are known. The upcoming instruments like LSST(Large Synoptic Survey Telescope) are likely to increase the number of lensed systems by atleast an order of magnitude and hence the number of higher order caustics will also increase. This project aims to assess the probability of estimating the gravitational potential of distant galaxy clusters by identification of these higher order caustics. This report discusses the gravitational lensing and the formation of caustics from a theoretical point of view. We have developed a numerical technique to estimate the caustics of different order for an arbitrary potential. We also have investigated image configurations corresponding to different lensing potentials using this numerical scheme.

1.1   Effect of gravity on radiation

A simple argument as explained below can demonstrate to us that how clock rates are affected by gravity. Consider the case, when in a weak gravitational field (hence, Newtonian gravity can be applied) a laser is being pointed towards the ground from a certain height L. Let us for the sake of argument, consider that the photons which carry the energy of this laser are converted to electron-positron pair. We shall consider the case of a single photon here, rest have similar fate. When this pair reaches the ground it gains an additional energy as it is comes to a place with less gravitational potential, hence, $h\nu = E_{down} = E_{up} + mgL$. Let us consider now that this pair is converted back to photon and sent up to the same height L. Now if we assume that the frequency of the photon has remained unchanged in this process then it means that every time the photons go up they gain an additional energy of

mgL. This violates the law of conservation of energy. If we rather consider that the frequency of photon should change as it travels through gravitational fields, this phenomena can be explained provided this change is given as

$$
\begin{aligned}
h\nu_{down} &= h\nu_{up} + mgL \\
&= h\nu_{up} + \frac{h\nu_{up}}{c^2} gL \\
&= h\nu_{up} \left(1 + \frac{gL}{c^2}\right)
\end{aligned}
\tag{1.1}
$$

In general, in a weak gravitational field having potential ϕ, we get

$$
\nu = \nu_o (1 - \frac{\phi}{c^2})
\tag{1.2}
$$

This simple analysis demonstrates the effect of gravity on the propagation of light rays. In this section we shall discuss this formally with help of General Theory of Relativity (GTR).

1.1.1 Line element in presence of weak gravitational field

Non-Relativistic action function for a particle in weak gravitational field ϕ has the form:

$$
A = -mc \int \left(c - \frac{v^2}{2c} + \frac{\phi}{c}\right).
\tag{1.3}
$$

Comparing this with the general action expression $A = -m \int ds$, we may get the interval as

$$
ds^2 = (c^2 + 2\phi)dt^2 - dr^2,
\tag{1.4}
$$

when $vdt = dr$. This suggests that for the weak gravitational potential, $g_{00} = (1 + 2\frac{\phi}{c^2})$, a result which shall be used often in the following sections.

1.1.2 Maxwell's Equations in weak gravitational field

Propagation of light in classical mechanics is governed by the Maxwell's equations. In this section we find the Maxwell's equations in a weak gravitational field. Electromagnetic field tensor is defined in flat space as

$$
F_{ik} = \frac{\partial A_k}{\partial x^i} - \frac{\partial A_i}{\partial x^k}
\tag{1.5}
$$

It is important to note that this definition remains invariant even in curvilinear coordinates because of the fact that Γ's are anti symmetric tensor.

$$F_{ik} = A_{k;i} - A_{i;k} = \frac{\partial A_k}{\partial x^i} - \frac{\partial A_i}{\partial x^k} \tag{1.6}$$

As a result the first pair of Maxwell's relations remain unchanged.

$$\frac{\partial F_{ik}}{\partial x^l} + \frac{\partial F_{li}}{\partial x^k} + \frac{\partial F_{kl}}{\partial x^i} = 0 \tag{1.7}$$

However, as the second pair of Maxwell's equation involve the current four vector, they need to be modified.

In case of a general coordinate with a the charge density ρ, the current four vector is given as

$$j^i = \frac{\rho c}{\sqrt{g_{00}}} \frac{dx^i}{dx^0}. \tag{1.8}$$

Therefore the remaining Maxwell relations can be written as

$$\frac{\partial_i \left[F^{ik} \sqrt{-g} \right]}{\sqrt{-g}} = \frac{4\pi}{c} j^i. \tag{1.9}$$

1.1.3   Effective refractive index

Considering the case of static gravitational field i.e. $g_{0\alpha} = 0$ and defining the quantities as follows:

$$E_\alpha = F_{0\alpha} \; , \; D^\alpha = -\sqrt{g_{00}} F^{0\alpha} \tag{1.10}$$

$$B_{\alpha\beta} = F_{\alpha\beta} \; , \; H^{\alpha\beta} = \sqrt{g_{00}} F^{\alpha\beta} \tag{1.11}$$

and using $\gamma_{\alpha\beta} = -g_{\alpha\beta}$ we can derive the following relations

$$D_\alpha = \frac{E_\alpha}{\sqrt{g_{00}}} \tag{1.12}$$

$$B^{\alpha\beta} = \frac{H_{\alpha\beta}}{\sqrt{g_{00}}}. \tag{1.13}$$

The above two equations represent the Maxwell's equations in 3 dimensional form in a static gravitational field. Comparing above equations with the case of electric amd magnetic fields inside an dielectric medium we may write, $\mu = \epsilon = \frac{1}{\sqrt{g_{00}}}$ and refractive index of gravity $n = g_{00} = (1 + 2\frac{\phi}{c^2})$. This indicates that the problem of lensing by a static gravitational field can be addressed in terms of ordinary optics. We shall use this formalism throughout the lensing theory. We shall only consider the cases of the static gravitational field here.

1.2   Theory of Gravitational Lensing

The order of magnitudes of distances between a source and a lens is generally much larger than that of the diameter of the galaxy or the cluster which act as a lens. As a result of which it is only important to study the defection within a thin zone close to the lens. Also, as we consider weak gravitational field we may use the effective Newtonian potential of the lens mass distribution here. In such a case, it is possible to assume that the the lensing mass is concentrated in a region and then estimate the gravitational field for that at different points (Gauss's law). First we shall consider the case of lensing by a point mass. Incidentally, the first ever theoretical understanding of the lensing by Einstein was also done by considering a point mass of a star. We shall develop the basic formalism here using the point mass approximation.

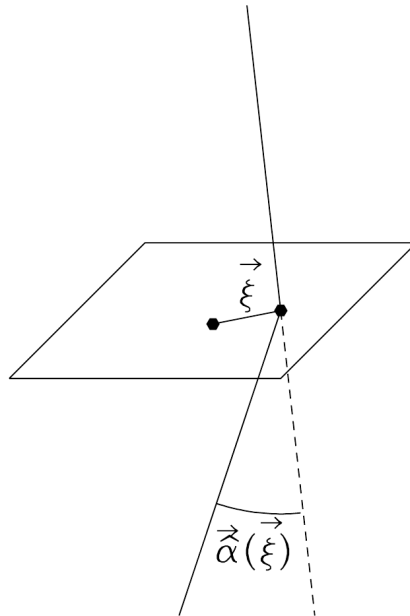**Thin screen approximation**

Figure 1.1: Thin screen approximation. Ref:[7]

We consider the case of a locally Minkowskian space time weakly perturbed by

the gravitational potential ϕ. Using the formalism developed in the previous section effective refractive index of gravitational field is

$$n = \left[1 + 2\frac{|\phi|}{c^2}\right]. \tag{1.14}$$

This apparently slows down the light rays in the gravitational field and former travels with a velocity v of

$$v = \frac{c}{n} \tag{1.15}$$

This reduction in speed amounts to a delay in arrival time of signal through the medium relative to that in vacuum. The total time delay, called the Shapiro's delay, can be calculated as

$$\Delta t = \int_{\text{source}}^{\text{observer}} \frac{dl}{v} - \frac{dl}{c} \tag{1.16}$$

$$= \frac{2}{c^3} \int dl \, |\phi|.$$

It is easy to see that the effective refractive index is a function of the position and hence n has a finite gradient. Like in optics, this non vanishing gradient causes deflection of light rays in the gravitational field. Deflection angle is equal to the integral along the light path of the gradient of n perpendicular to light path. However, as we are considering the case of a weak gravitational potential, the deflection angle is small the above integration can be done along an unperturbed ray instead of the deflected ray but with the same impact parameter:

$$\vec{\hat{\alpha}} = -\int \vec{\nabla}_\perp n \, dl = \frac{2}{c^2} \int \vec{\nabla}_\perp \Phi \, dl. \tag{1.17}$$

Clearly, what remains is to calculate the gravitational potential for a given mass distribution. As the extent of the lens is very small compared to both the source-lens and the lens-observer distance, it is often customary to assume that all the deflection due to gravity occurs only at the lens position. This is analogus to the thin lens approximation considered in ordinary optics and makes the above integral quite straight forward. Figure 1.1 shows a light ray deflecting close to the lens plane. In mathematical terms, mass distribution of the lens can then be projected along the line of sight and replaced by a mass sheet (often called the lens plane) orthogonal to the sight line. The important quantity that comes into the deflection integral then is the surface mass density of this mass sheet defined as $\Sigma(\varepsilon) = \int \rho(\varepsilon, z) dz$. Here ε

is the two-dimensional vector in the lens plane. The net deflection angle is equal to the contributions from all the mass elements in the lens plane and is given as:

$$\vec{\hat{\alpha}} = \frac{4G}{c^2} \int \frac{(\varepsilon - \vec{\varepsilon'})\Sigma(\vec{\varepsilon'})}{\mid \varepsilon - \vec{\varepsilon'} \mid^2} d^2\varepsilon' \tag{1.18}$$
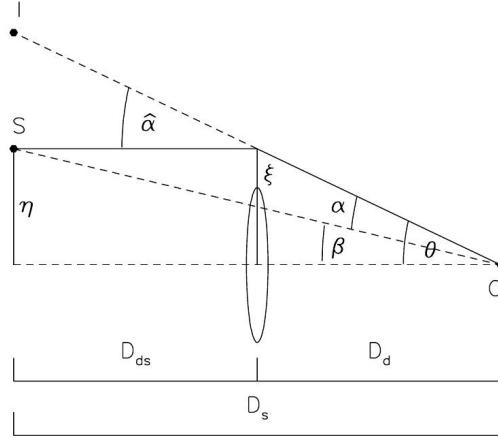
Figure 1.2: Lensing Geometry[7]

Lensing Geometry

Figure 1.2 demonstrates the overall geometry of a gravitational lens system. The angle between the arbitrarily chosen optic axis and the source position S is $\vec{\beta}$ and between the optic axis and image I is $\vec{\theta}$. The quantities D_d, D_{ds} and D_s represent the angular diameter distances between the observer and the lens, lens and source, and observer and source. It is customary to define reduced deflection angle as: $\vec{\alpha} = \frac{D_{ds}}{D_s}\vec{\hat{\alpha}}$. From simple geometry we can see that

$$\vec{\beta} = \vec{\theta} - \vec{\alpha(\vec{\theta})}. \tag{1.19}$$

This equation forms the foundation of Gravitational Lensing and is known as the **lens equation**. Observationally, one has the information of the image positions θ. Solving the lens equation, the source position β is inferred. For a circularly symmetric lens the magnitude of the deflection angle is

$$\hat{\alpha(\varepsilon)} = \frac{4GM(\varepsilon)}{c^2\varepsilon} \tag{1.20}$$

where ε is the distance from the center of the lens and $M(\varepsilon)$ is the mass enclosed within the radius ε,

$$M(\varepsilon) = 2\pi \int_0^{\varepsilon} \sum(\varepsilon')\varepsilon'd\varepsilon'. \tag{1.21}$$

It is clear that by measuring the deflection angle from observations one can estimate the mass responsible for lensing.

Critical Density

Unlike optical lenses, gravitational lenses do not always have a definite focal length. Result is that for gravitational lenses, light from the source is not directed towards the observer, or focused at the observer. For the focusing effect to occur, the lens must have a particular density, namely the critical density. To understand the concept of critical density let us consider a special case of lens having constant surface mass density, the reduced deflection angle then becomes

$$\alpha(\vec{\theta}) = \frac{D_{ds}}{D_s}\frac{4G}{c^2\varepsilon}(\Sigma\pi\varepsilon^2) = \frac{4\pi G\Sigma}{c^2}\frac{D_{ds}D_d}{D_s}\theta \tag{1.22}$$

where $\varepsilon = D_d\theta$. Now, to make all the light rays come to observer, we essentially need $\beta = 0$, i.e. $\alpha(\theta) = \theta$. The surface mass density required for this to happen is called the critical mass density Σ_{cr}, hereby,

$$\Sigma_{cr} = \frac{c^2}{4\pi G}\frac{D_s}{D_d D_{ds}}. \tag{1.23}$$

Clearly, a typical lens in general will show a different behavior. The light rays with different impact parameter will be deflected at different angles. Multiple images occur if the lens is super critical i.e. $\Sigma > \Sigma_{cr}$.

Einstein Radius

Writing the lens equation for a circularly symmetric lens with an arbitrary mass profile we get

$$\beta(\theta) = \theta - \frac{D_{ds}}{D_d D_s}\frac{4GM(\theta)}{c^2\theta} \tag{1.24}$$

For a source at the axis ($\beta = 0$) the image is a ring with a radius

$$\theta_E = \left[\frac{4GM(\theta)}{c^2}\frac{D_{ds}}{D_d D_s}\right]^{1/2} \tag{1.25}$$

if the lens is super critical. Hence, for a source at the center the image is a ring, this ring is called as the Einstein ring and the radius θ_E is called the Einstein radius. The value of θ_E in case of the lensing by a star of mass $M \sim M_\odot$ and $D \sim \frac{D_d D_{ds}}{D_s} = 10$ kpc $\theta_E = 0.9$ micro arc seconds while for a galaxy of mass $M \sim 10^{11} M_\odot$ and $D \sim 1$ Gpc $\theta_E = 0.9$ arc seconds. It is important to note that Einstein radius is not only the property of the lens but it also depends on the different distances involved in the problem. For a given lens mass and D_s deflection is largest when $D_s = D_{ds}$.

1.2.1   Properties of images

Magnification

The most important property of images formed as a result of lensing is that they are highly magnified. This is because surface brightness is preserved in the case of gravitational deflection while the apparent solid angle of the source changes. Hence

$$\text{magnification} = \frac{\text{image area}}{\text{source area}} \tag{1.26}$$

Clearly, using the lensing geometry, for a circularly symmetric lens, the magnification factor is

$$\mu = \frac{\theta}{\beta}\frac{d\theta}{d\beta}. \tag{1.27}$$

In absence of symmetry we can see it as a mapping of a solid angle element of the source $\delta\beta^2$ to the solid angle element of the image $\delta\theta^2$.

Achromatism

We have defined the effective refractive index of the light rays in the gravitational field considering parallelism with ordinary optics. However, as the effective refractive index here depends only on the geometry of the space-time or the gravitational field, it has no dependence on the wavelength of radiation considered. Hence, the gravitational lenses, unlike optical lenses, have no chromatic aberration.

1.2.2   Imaging by a point mass lens

In this section we discuss the simple case of imaging by a point mass lens. For a point mass Einstein radius is

$$\theta_E = \frac{4GM}{c^2} \frac{D_{ds}}{D_d D_s} \tag{1.28}$$

The lens equation then becomes:

$$\beta = \theta - \frac{(\theta_E)^2}{\theta}. \tag{1.29}$$

As above is a quadratic equation, it has two solutions and two images are formed with positions at

$$\theta_\pm = \frac{1}{2}(\beta \pm \sqrt{\beta^2 + 4\theta_E^2}). \tag{1.30}$$

The magnification of the two images are

$$\mu_\pm = \left[1 - \left(\frac{\theta_E}{\theta_\pm}\right)^4\right]^{-1} = \frac{u^2 + 2}{2u\sqrt{u^2 + 4}} \pm \frac{1}{2}, \tag{1.31}$$

where u is the angular separation of the source from point mass in units of Einstein radius. The two images are located on either side of the source, with one image inside the Einstein ring and the other outside. For $\theta < \theta_E$, $\mu_- < 0$ i.e Image inside the Einstein ring has negative magnification. The interpretation of negative μ is that parity of the image is flipped with respect to the source. The net magnification of the images is

$$\mu_{net} = \mid \mu_+ \mid + \mid \mu_- \mid = \frac{u^2 + 2}{u\sqrt{u^2 + 4}} \tag{1.32}$$

1.2.3   Imaging by a Singular Isothermal sphere

In this section we consider lensing by galaxies where the model for mass distribution in galaxies is that of a singular isothermal sphere. The density is given by:

$$\rho(r) = \frac{\sigma_v^2}{2\pi G} \frac{1}{r^2}. \tag{1.33}$$

This mass distribution is called the singular isothermal sphere($\rho \propto r^{-2}$). As a result, the mass $M(r) \propto r$ and the rotational velocity of particles

$$v_{rot}^2(r) = \frac{GM(r)}{r} = 2\sigma_v^2 = \text{constant} \tag{1.34}$$

Upon projecting the mass density along the line of sight we get the surface mass density as

$$\Sigma(\varepsilon) = \frac{\sigma_v^2}{2G}\frac{1}{\varepsilon}, \tag{1.35}$$

where ε is the distance from the center of the two dimensional profile. Deflection angle is

$$\hat{\alpha} = 4\pi\frac{\sigma_v^2}{c^2}, \tag{1.36}$$

which is independent of ε. The Einstein radius is :

$$\theta_E = 4\pi\frac{\sigma_v^2}{c^2}\frac{D_{ds}}{D_s} = \alpha. \tag{1.37}$$

The lens equation gives two solutions

$$\theta_\pm = \beta \pm \theta_E \tag{1.38}$$

The magnifications of two images are

$$\mu_\pm = \frac{\theta_\pm}{\beta} = 1 \pm \frac{\theta_E}{\beta} = (1 \mp \frac{\theta_E}{\theta_\pm})^{-1} \tag{1.39}$$

On careful consideration it can be seen that a third image with zero flux is situated at $\theta = 0$. Multiple images are obtained if $\beta < \theta_E$. If the source lies outside the Einstein ring, there is only one image at $\theta = \theta_+ = \beta + \theta_E$. This suggests that the Einstein's ring defines two different regions in the source plane, and this shall be the centre of our discussion at a later section.

Chapter 2

Mathematical formalism of Gravitational lensing

In this chapter we describe the general analytical formalism of lensing problem and discuss a few examples.

2.0.4 Effective Lensing Potential

In this section we develop a formalism to describe image formation by an arbitrary lens model. We define a scalar potential $\psi(\vec{\theta})$ which is the scaled, projected Newtonian potential of the lens:

$$\psi(\vec{\theta}) = \frac{D_{ds}}{D_d D_s} \frac{2}{c^2} \int \Phi(D_d\vec{\theta}, z)dz \tag{2.1}$$

$$\vec{\nabla}_\theta \psi = D_d \vec{\nabla}_\varepsilon \psi = \frac{D_{ds}}{D_s} \frac{2}{c^2} \int \vec{\nabla}_\perp \Phi dz = \vec{\alpha} \tag{2.2}$$

$$\nabla_\theta^2 \psi = \frac{2}{c^2} \frac{D_{ds}}{D_d D_s} \int \nabla_\varepsilon^2 \Phi dz = \frac{2}{c^2} \frac{D_{ds}}{D_d D_s} 4\pi G\Sigma = 2\frac{\Sigma(\vec{\theta})}{\Sigma_{cr}} = 2\kappa(\vec{\theta}) \tag{2.3}$$

The last expression makes use of the Poisson's equation to relate the Laplacian of Φ to the mass density. The scaled projected density divided by the critical density $\kappa(\vec{\theta})$ is called the convergence.

The lens mapping can be described by the Jacobian matrix

$$A = \frac{\partial\vec{\beta}}{\partial\vec{\theta}} = \left[\delta_{ij} - \frac{\partial\alpha_i(\vec{\theta})}{\partial\theta_j}\right]. \tag{2.4}$$

Using $\vec{\nabla}_\theta \psi = \vec{\alpha}$ we get,

$$A = \left[\delta_{ij} - \frac{\partial^2 \psi(\vec{\theta})}{\partial\theta_i \partial\theta_j}\right] = M^{-1} \tag{2.5}$$

A is also called the inverse magnification tensor (M). The distortion in solid angle is given by the determinant of A. It can be clearly seen from equation 2.5 that the matrix of second partial derivatives of potential ψ describes the deviation of the lens mapping from identity.

Using $\frac{\partial^2 \psi(\vec{\theta})}{\partial\theta_i \partial\theta_j} = \psi_{ij}$

$$\kappa = \frac{1}{2}(\psi_{11} + \psi_{22}) = \frac{1}{2} Tr \; \psi_{ij} \tag{2.6}$$

Components of shear tensor can be written as

$$\gamma_1(\vec{\theta}) = \frac{1}{2}(\psi_{11} + \psi_{22}) = \gamma(\vec{\theta})cos\left[2\phi(\vec{\theta})\right] \; , \tag{2.7}$$

$$\gamma_2(\vec{\theta}) = \psi_{12} = \psi_{21} \equiv \gamma(\vec{\theta})sin\left[2\phi(\vec{\theta})\right] . \tag{2.8}$$

Jacobian matrix is given by

$$\begin{aligned} A &= \begin{pmatrix} 1 - \kappa - \gamma_1 & -\gamma_2 \\ -\gamma_2 & 1 - \kappa + \gamma_1 \end{pmatrix} \\ &= (1-\kappa)\begin{pmatrix} 1 & 0 \\ 0 & 1 \end{pmatrix} - \gamma\begin{pmatrix} cos2\phi & sin2\phi \\ sin2\phi & -cos2\phi \end{pmatrix} \end{aligned} \tag{2.9}$$

Physically convergence means an isotropic magnification of source(for example a circle transforming to a circle with larger radius) while shear introduces anisotropy into the mapping(a circle transforming to an ellipse). γ is the magnitude of shear and ϕ describes the orientation.

$$\mu = detM = \frac{1}{detA} = \frac{1}{[(1-\kappa)^2 - \gamma^2]} \tag{2.10}$$

2.0.5   Formation of images: Fermat's principle

Time -Delay function

The lens equation can be cast in the form

$$\vec{\nabla}_\theta\left[\frac{1}{2}(\vec{\theta} - \vec{\beta})^2 - \psi\right] = 0 \tag{2.11}$$

The term in the parenthesis can be recognized as the time delay function,

$$t(\vec{\theta}) = \frac{(1+z_d)}{c}\frac{D_dD_s}{D_{ds}}\left[\frac{1}{2}(\vec{\theta}-\vec{\beta})^2 - \psi(\vec{\theta})\right] \tag{2.12}$$
$$= t_{geom} + t_{grav}.$$

The term t_{geom} represents the time delay due the geometric path difference relative to the unperturbed light ray while the term t_{grav} is the Shapiro's delay that we have encountered before. The coefficient in the front ensures that this corresponds to time delay as measured by the observer. Using Fermat's principle we can write

$$\vec{\nabla}_\theta t(\vec{\theta}) = 0 \tag{2.13}$$

Like conventional lenses images will form at extrema in the light travel time surface. These extrema/stationary points of a two dimensional surface are of three types: maxima, minima and saddle points [**?**]

$$T = \frac{\partial^2 t(\vec{\theta})}{\partial\theta_i\partial\theta_j} = (\delta_{ij} - \psi_{ij}) = A \tag{2.14}$$

The matrix T describes the local curvature of time-delay surface. The classification of stationary points is on the basis of following criteria:

- If both the eigen values of T are negative i.e.where $detA > 0$ and $trA < 0$, the stationary point is a maxima.

- If both the eigen values of T are positive i.e.where $detA > 0$ and $trA > 0$, the stationary point is a minima.

- If both the eigen values of T have opposite signs i.e.where $detA < 0$, the stationary point is a saddle .

Since magnification is inverse of $detA$ images of type1 and 2 have positive magnification while images of type 3 have negative magnification or the parity of the image is reversed. VLBI observations have shown that this is indeed true.

Critical curves and caustics

Critical curves are curves in θ space (image plane) where $detA = 0$. Corresponding curves in β space (source plane) are called caustics. It is possible to look at critical curves and caustics in terms of magnification. These are curves of infinite magnification i.e. $detM = \frac{1}{detA} \to \infty$. They are of great importance because

1. They highlight regions of high magnification.

2. They demarcate the regions of different image multiplicity.

Four commonly used circularly symmetric lens models are :

- Point mass

- Constant Density sheet

- Singular Isothermal sphere

- Softened Isothermal sphere

2.1   Circularly Symmetric Lens Models

The image configurations produced by circularly symmetric lenses can be found out with the knowledge of time delay functions $t(\theta)$ vs θ. The figure below shows time delay function of a circularly symmetric lens for a source at a slightly offset position. The dotted line shows the location of the center of the lens and β shows the position of the source.
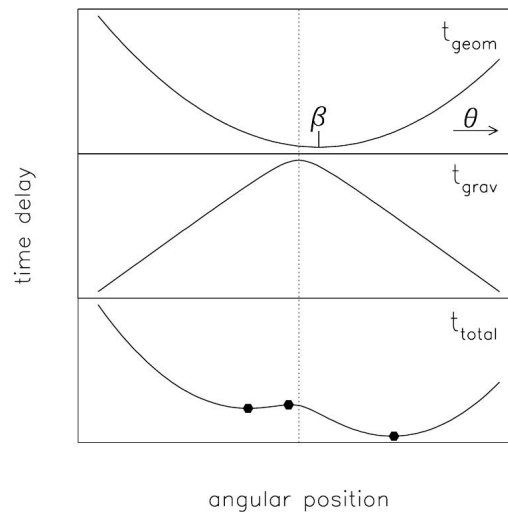

Figure 2.1: Time delay function vs θ for an offset source [7]

2.1.1 Softened Isothermal Sphere

First three lens models have been discussed in the previous sections, therefore this section elaborates the analysis of softened isothermal sphere. The projected scalar potential in this case is given by

$$\psi(\theta) = \frac{D_{ds}}{D_s} \frac{4\pi\sigma^2}{c^2} (\theta_c^2 + \theta^2)^{1/2} \tag{2.15}$$

where θ_c is the softening radius. Therefore

$$\alpha(\theta) = \frac{D_{ds}}{D_s} \frac{4\pi\sigma^2}{c^2} \frac{\theta}{(\theta_c^2 + \theta^2)^{1/2}} \tag{2.16}$$

The lens equation is :

$$\beta = \theta(1 - \frac{K}{(\theta_c^2 + \theta^2)^{1/2}}) \tag{2.17}$$

where $K = \frac{D_{ds}}{D_s} \frac{4\pi\sigma^2}{c^2}$ Since $det A = \frac{\beta}{\theta} \frac{\partial\beta}{\partial\theta}$

$$\frac{\partial\beta}{\partial\theta} = 1 - \frac{K\theta_c^2}{(\theta_c^2 + \theta^2)^{3/2}} \tag{2.18}$$

$$det A = \left(1 - \frac{K}{(\theta_c^2 + \theta^2)^{3/2}}\right)\left(1 - \frac{K\theta_c^2}{(\theta_c^2 + \theta^2)^{3/2}}\right)$$

Equating $det A$ to zero we get the following critical curves and caustics :

$$\theta = \sqrt{K^2 - \theta_c^2}, \quad \beta = \theta - \frac{K\theta}{K} = 0 \tag{2.19}$$

$$\theta = (K\theta_c^2)^{2/3} - \theta_c^2, \quad \beta = \theta(1 - (\frac{K}{\theta_c})^{2/3} \tag{2.20}$$

$$= (K^{2/3} - \theta_c^{2/3})^{3/2} \tag{2.21}$$

The graph shown in figure (2.2) plots β vs θ for different values of softening radius. The green curve($\theta_c = 0$) represents the case of singular isothermal sphere discussed in previous sections. The two extrema points are the critical points as shown in above calculations. Clearly for any $\theta < \theta_c$ there are three images corresponding to three values of β while for any value of $\theta > \theta_c$ only one image can be seen. To have a better understanding of the position of images with respect to the critical curves, β vs θ (2.3)) is plotted for a fixed value of softening radius. The gray and black circles represent the caustic and critical curve respectively. The position of the images (intersection of green line with the blue curve) can then be located with respect to these curves.
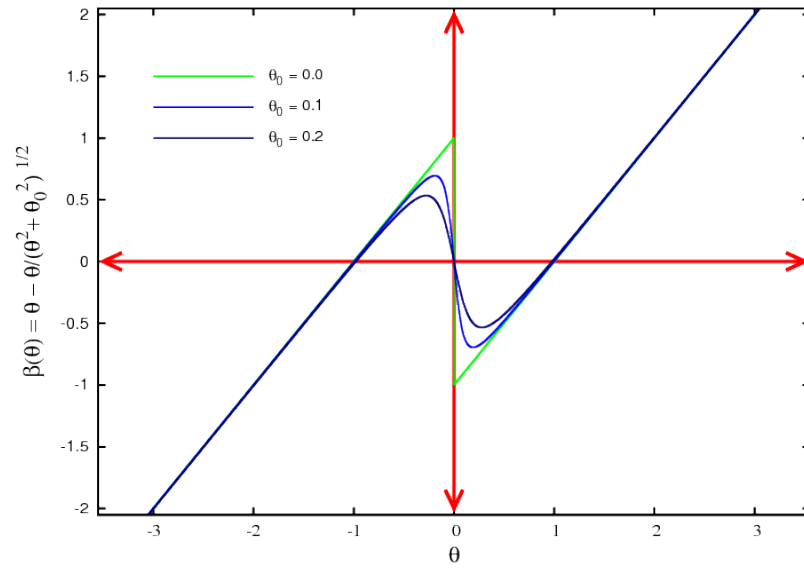
Figure 2.2: β vs θ different values of softening radius

Figure 2.3: β vs θ.
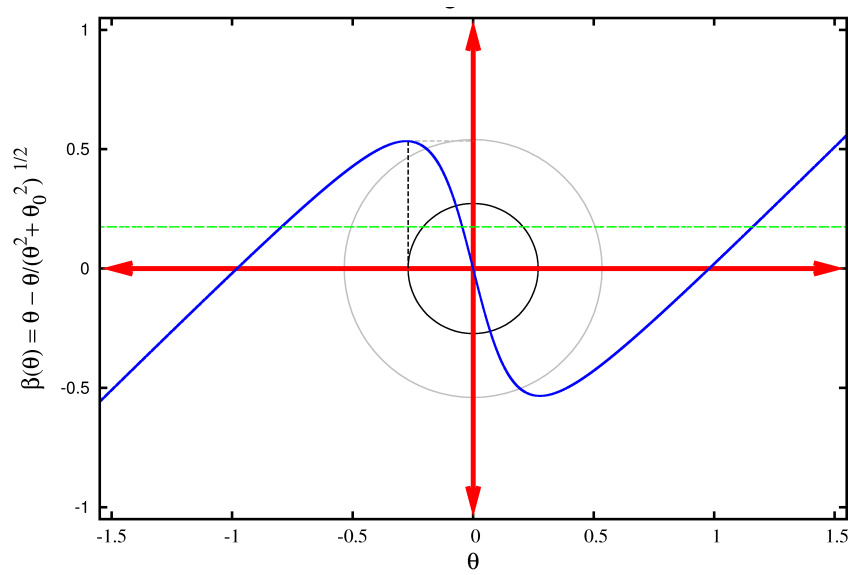
Chapter 3

Different lens models: A numerical study

In this project we study the image configurations for different lens models and investigate the lens singularities. Our aim is to produce a database of possible lensing scenarios such that it is possible to identify them with the help of the upcoming surveys like LSST. It is well known that with help of first order singularities in the image, it is not possible to reconstruct the lensing potential unambiguously. We investigate the higher order singularities in this chapter. We shall consider the simple lensing potentials first and then move onto more complex lens models. We first describe the procedure adopted for this study and then consider different examples. Our approach is two fold here. First we investigate the possible singularities in a given lens model. Then we consider different source positions and numerically estimate the image positions for each of them. Here we summarise the steps

1. To start with, we choose a form of the lensing potential $\psi(\vec{\theta})$. Here $\vec{\theta}$ is the angular vector in the sky corresponding to any observation centre. Main resources for this exercise are the functional form of the potential and the lens equation given by

$$\vec{\beta} \; = \; \vec{\theta} - \nabla \psi \tag{3.1}$$

We define this potential on a rectangular grid and proceed further. It is important to note that since we define the potential in a grid, it is possible in principle to adopt the following steps for any arbitrary potential.

2. We numerically compute the Eigen values and Eigen vectors of $\psi_{ij} = \frac{\partial^2 \psi}{\partial \theta_i \partial \theta_j}$. To do this we need to evaluate second derivative of the potential at each grid point. As this is the first numerical method we have used here, any numerical error in this step is expected to carry over and multiply in the further stages. Hence we have used a second order accurate five point finite difference scheme to estimate the derivatives. As the projected potential is defined in two dimensions, we have two sets of Eigen values and Eigen vectors at each grid point. We denote the Eigen values as λ_1, λ_2 and the eigen vectors as $\hat{\mathbf{e}}_1$ and $\hat{\mathbf{e}}_2$. After these steps the numerical values of λ's and $\hat{\mathbf{e}}$'s at each grid point are stored in appropriate arrays.

3. We search for different lens singularities using Eigen values and Eigen vectors. Specifications are discussed below. Similar mathematical structures are discussed in [1] in the context of gravitational clustering, interesting readers may look in it.

   - **Critical curves and Caustics**: Critical curves are defined to be the curves in the image plane where at least either of the Eigen values of the matrix ψ_{ij} is unity, i.e, $(1 - \lambda_1)(1 - \lambda_2) = 0$. We search for points where this condition is satisfied in the image plane by interpolating from the gridded Eigen values. The corresponding lines in the source plane are called the caustics.

   - **Cusps, Folds and A3 lines**: Cusps and folds are special types of critical curves. A fold is formed when a segment of a critical curve maps to a smooth curve in a sorce plane. On the other hand cusps form when an infinitesimal segment of a critical curve maps to a point in the source plane. Cusps lie on A3 lines which are formed where the following criteria is satisfied:

     $$\nabla \lambda . \hat{\mathbf{e}} = 0. \tag{3.2}$$

     We numerally investigated the criteria for A3 lines by interpolating these values at different grid points.

   - **Unstable fixed points, A4 and D4:** All the singularities described till now are stable singularities. This implies that on changing the parameters of the model lens, the singularities shift though their nature remain

the same.We have investigated unstable singularities. The advantage of analysing the unstable singularities lies in the fact that they produce special image configurations only for very specific values of the lens parameters. Hence observing image configurations near these points gives us knowledge about the lens parameters. Here we discuss the analysis of two different unstable singularities.

A4 points are defined to be points where the tangent to the A3 line has the same direction as the Eigen vector at that point. D4 points are defined to be the points where two Eigen values of the matrix A are equal. These points are found at very specific values of the lens parameters. We shall discuss it with an example in the next section.

4. We consider a single circular source at the background of the lens and simulate the image configurations for different positions of the source provided a lensing potential. We then use ray shooting method to calculate the image positions from the lens equation. We briefly describe the ray shooting method as follows.

Ray shooting method: Ray shooting methodis used to locate points in the image plane corresponding to a source position and geometry for a particular lensing potential. The analytical form of the lens equation allow us to calculate the source position directly if the image position is known. Using this method we proceed in the following way. We divide the image plane into a rectangular grid. For each grid point, we numerically calculate the corresponding source position using the lens equation. Then we check if the position obtained in the source plane by this method is consistent with the position of the source in consideration. If affirmative, we print the source and the image positions, else we discard the image position. We repeat this for all the grid points in the image plane. It is important to note that for this method to work the extent of the image plane has to be large enough to fit all the image configurations inside it. On the other hand the grid size of the image plane decides the accuracy to which we can estimate the image positions. If the grid size does not have sufficient resolution, it is possible to merge two physically separate images. In principle a nested grid method can be applied. Here we have incorporated a single (1024×1024) gird to do the numerical calculations. This works well for

the potential we have studied so far.

3.1 Special cases of lens potentials

In this section we numerically calculate the critical curves and images for different lensing potentials. We also investigate the parameters of the lensing potentials that gives rise to the unstable singularities namely the A4 and D4 points.

3.1.1 Softened Isothermal Sphere

We have already discussed the softened isothermal sphere potential before, here we briefly mention the results for the critical curves and image configurations for different source positions. This potential is modeled after a galactic dark matter halo.

Effective Potential

$$\psi(\theta) \;=\; \frac{D_{ds}}{D_s} \frac{4\pi\sigma^2}{c^2} \left[\theta_c^2 + \theta^2 \right]^{1/2}, \tag{3.3}$$

here θ_c is the softening scale. Note that the angular diameter distances, D_{ds} and D_s depends on the redshift of the source and the lens. The parameters of this lens are the softening length θ_c, redshift to the source and the lens, and the velocity dispersion σ. Note that as the source passes a caustic, the number of images are increased or decreased by two. As the source approaches the centre, we see the formation of an Einstein ring.

Critical curves and images

Figure (3.1) shows the critical curves and caustics for this lens configuration. Image configurations for three different source positions are shown in Figure (3.2) .

3.1.2 Softened Isothermal lens: elliptical geometry

In an astrophysical situation, ellipsoidal lenses are more generic compared to the circularly symmetric cases. Here we generalise the softened isothermal lens with ellipsoidal geometry.
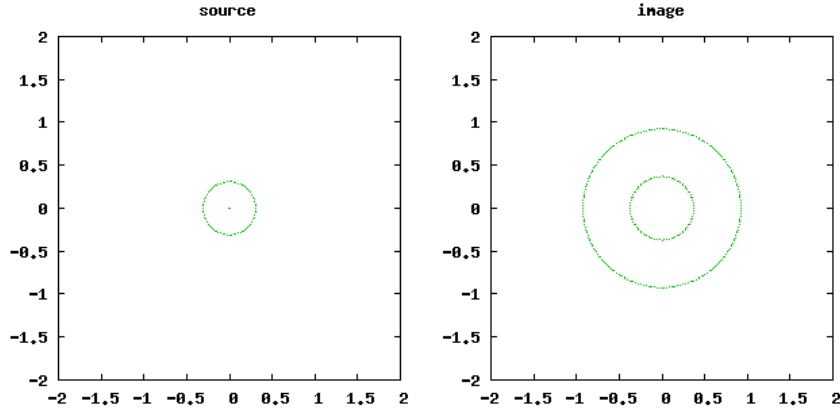
Figure 3.1: Critical curves and caustics for the softened isothermal sphere potential. Axis levels are arbitrary.

Effective Potential

$$\psi(\theta_x, \theta_y) \;=\; \frac{D_{ds}}{D_s} \frac{4\pi\sigma^2}{c^2} \left[\theta_c^2 + (1 - \epsilon)\theta_x^2 + (1 + \epsilon)\theta_y^2\right]^{1/2}, \tag{3.4}$$

where ϵ is the eccentricity of the ellipse.

Critical curves and images

Figure (3.3) shows the critical curves and caustics for this kind of lens configuration. Cusp and fold formation in the critical curves can be clearly seen. We investigate image formations when the source passes a cusp and fold in Figure (3.4) and Figure (3.5) respectively. We see that as the source approaches the caustics, the image becomes elongated (sheared) and breaks into three images as it passes the caustic. In case when the source passes the fold caustics, at the central position of the source, four broken arcs replace an Einstein ring along with a small central image. Figure (3.6) shows an observation of an image configuration by [2] using VLT at a redshift of 3.773. Their lens model is also shown in the same figure. Remarkable similarity of this image configuration with the third pannel of Figure (3.5) is noticable. Though it is not shown here, for small ellipticity and a little extended source, ellipse shaped Einstein ring can be still seen. When the source passes the cusp type caustic, at the central position an elongated arc like image is formed. Figure (3.7) shows the A3

lines in the image plane for this lens configuration.

Till now we have been investigating the stable lens singularities and hence a critical choice of the parameters was not necessary. We now investigate the D4 point for the present lens geometry. To do this we look at the evolution of the caustics and the critical curves for different distances between the source and the lens and seek for the particular value of the source to lens distance, for which the condition for D4 point (i.e, $\lambda_1 = \lambda_2$) is satisfied. As the angular diameter distance D_{ds} depends on the redshift of the source, we label the different distances as the corresponding different redshifts of the source. However one need to keep in mind that these redshifts are just to label different images and depends on other parameters of the lens. Figure (3.9) shows the critical curves and caustics for three different values of the redshifts. In the middle figure, we obtain the D4 point. An observation from the cluster Abell 1703 [8] is shown in the Figure (3.10), where image configuration similar to the bottom panel of Figure (3.8).

3.1.3   Softened Isothermal lens: two ellipse geometry

Next we consider the case when there are two softened isothermal elliptical lenses in the light path from source to the observer. This can be realised in nature as mergers of two clusters of galaxies. Therefore we choose the potential to have the following form.

Effective Potential

$$
\begin{aligned}
\psi(\theta_x, \theta_y) \quad = \quad & F_1 \left[\theta_{c_1}^2 + (1 - \epsilon_1)\theta_x^2 + (1 + \epsilon_1)\theta_y^2 \right]^{1/2} \\
+ \quad & F_2 \left[\theta_{c_2}^2 + (1 - \epsilon_2)(\theta_x' - \theta_{x0})^2 + (1 + \epsilon_2)(\theta_y' - \theta_{y0}),^2 \right]^{1/2}
\end{aligned}
\tag{3.5}
$$

where the parameters F_1 and F_2 depends on the redshift of the source and the lens, the velocity dispersions and the particular cosmology in consideration. Generically the parameters of such a lens can be wide fold, we consider only a set of parameters here that gives rise to a particulartype of caustics and critical curves. The quantities θ_x' and θ_y' are the rotated coordinates with respect to the coordinates θ_x and θ_y by an angle ϕ.

Critical curves and images

Critical curves and caustics are shown in the source and image planes along with the image formations for three different source positions in Figure (3.11). The parameters are adjusted so that the critical curve passes through the A4 point of the configuration. As the source passes through the corresponding point in the caustics, we see formation of straight arc like configuration. This is a very special signature of A4 type singularity as shown in the bottom panel of Figure (3.14) . We also show the A3 lines corresponding to this lens configuration in Figure (3.12) , where complicated geometry of the lens is reflected. The A4 point is marked by a orange dot in this plot.

Figure (3.13) shows four interesting A3 line configurations for different sets of lens parameters. Of particular interest is the bottom right figure, where a pyramid D4 point is formed. As clear from Figure (3.15)the three A3 lines corresponding to each eigen value merge at this point. We investigate image formations when the source passes a caustic at Pyramid D4 point in Figure (3.14).
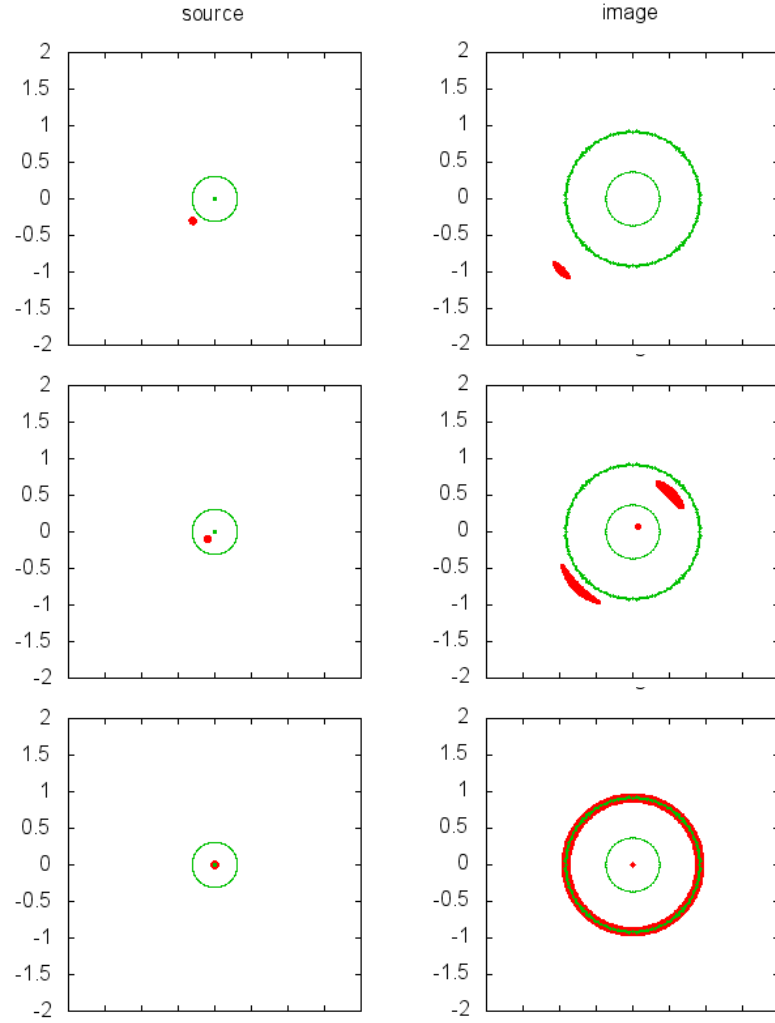
Figure 3.2: Image positions for three different source positions are shown for a softened isothermal sphere lens. Note that as the source passes a caustic, number of images change by 2. For the central position of the source, an Einstein ring is observed. Axis labels are arbitrary.
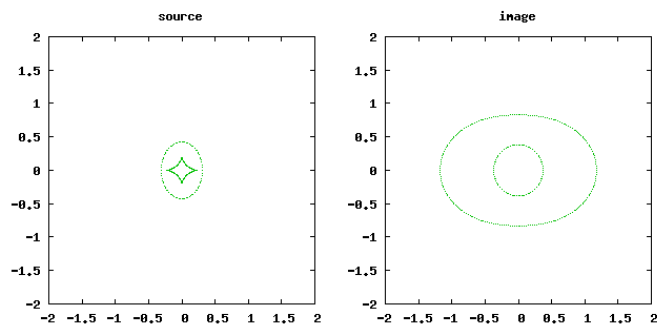
Figure 3.3: Critical curves and caustics for the soften isothermal lens with ellipsoidal symmetry potential. Axis levels are arbitrary.
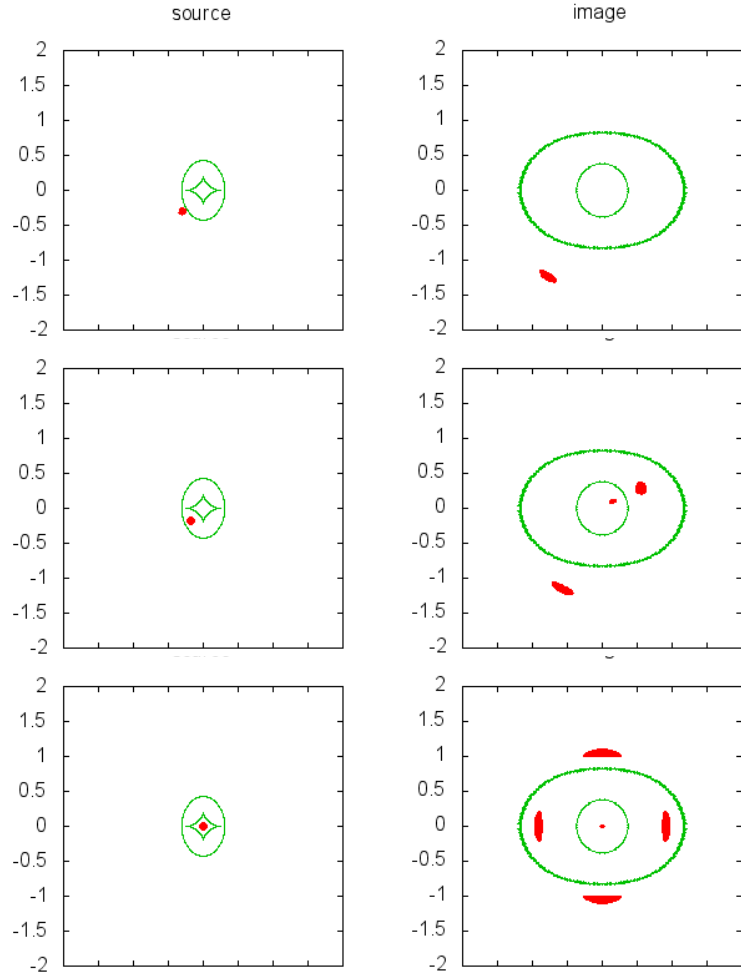
Figure 3.4: Image positions for three different source positions are shown for a softened isothermal spherical lens as the source passes a fold caustic. For the central position of the source now four distinct arcs are formed with a central small image.
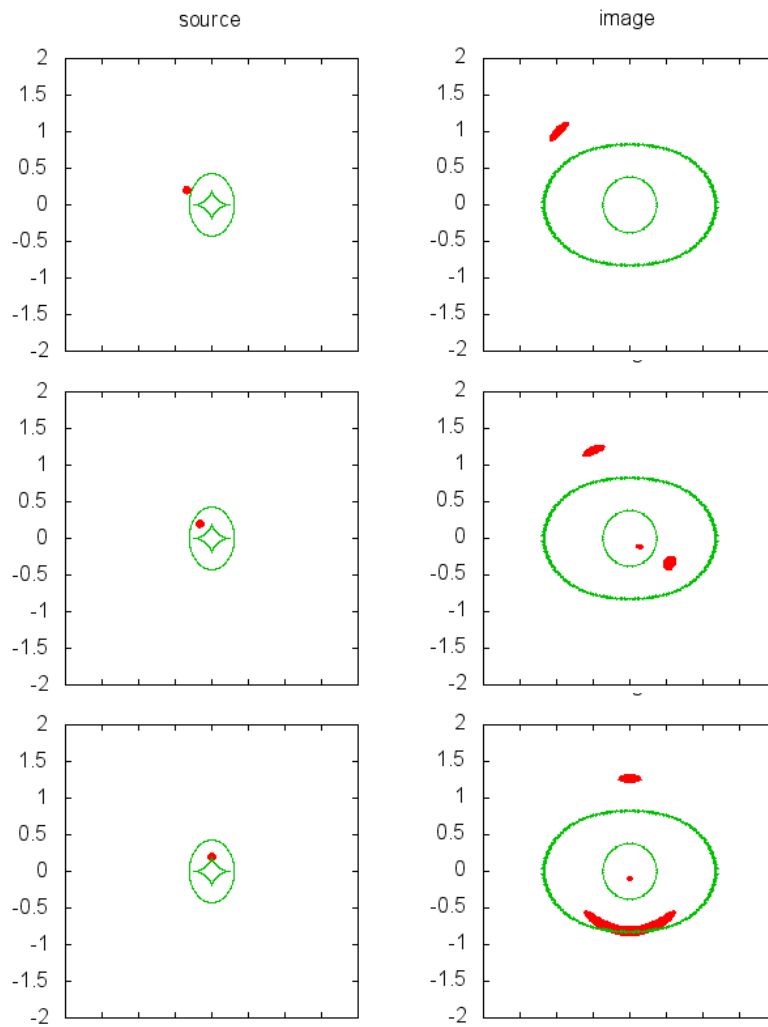
Figure 3.5: Image position for three different source positions are shown for a softened isothermal spherical lens as the source passes a cusp caustic. When the source is over the cusp, an elongated arc is created.
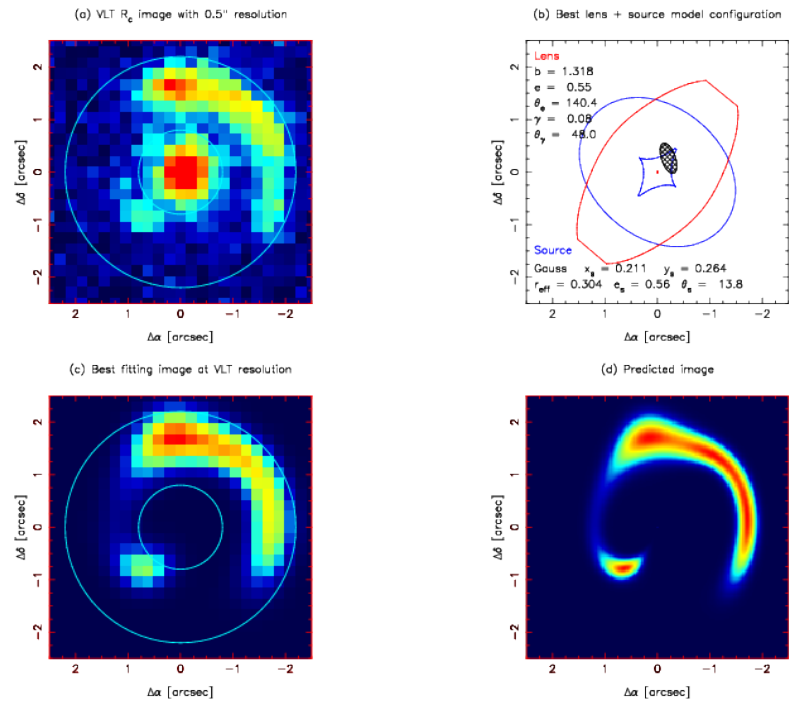
Figure 3.6: Image formation as the source passes through a cusp caustic reported by Cabanac et al. [2]. Top left to clockwise: VLT observed image, lens model with caustics, simulated image and simulated image in VLT resolution.
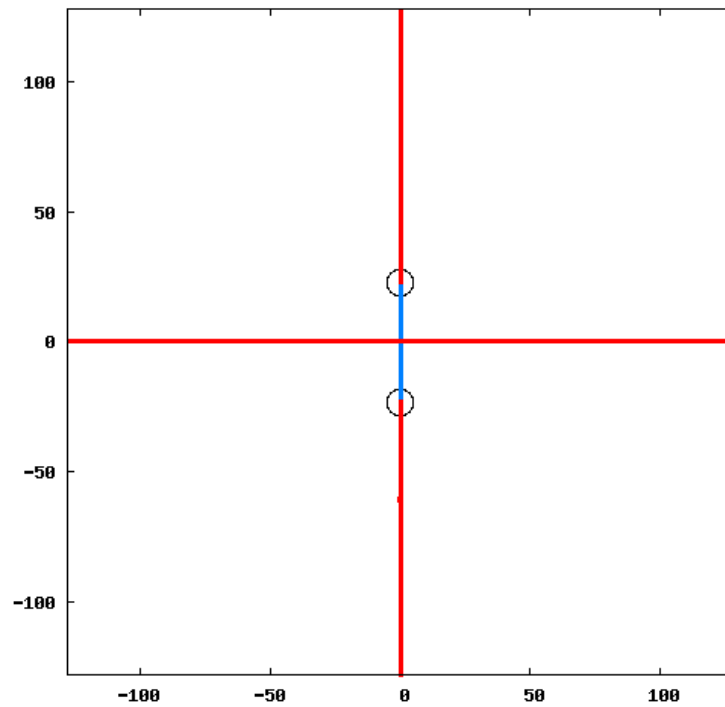
Figure 3.7: A3 lines for softened isothermal elliptical potential is shown. Two colors (red and magenta) give the A3 lines corresponding to two eigenvalues. Note that the axis labels are arbitrary. Points where A3 lines of two eigenvalues merge are the D4 points and they are marked using circles.
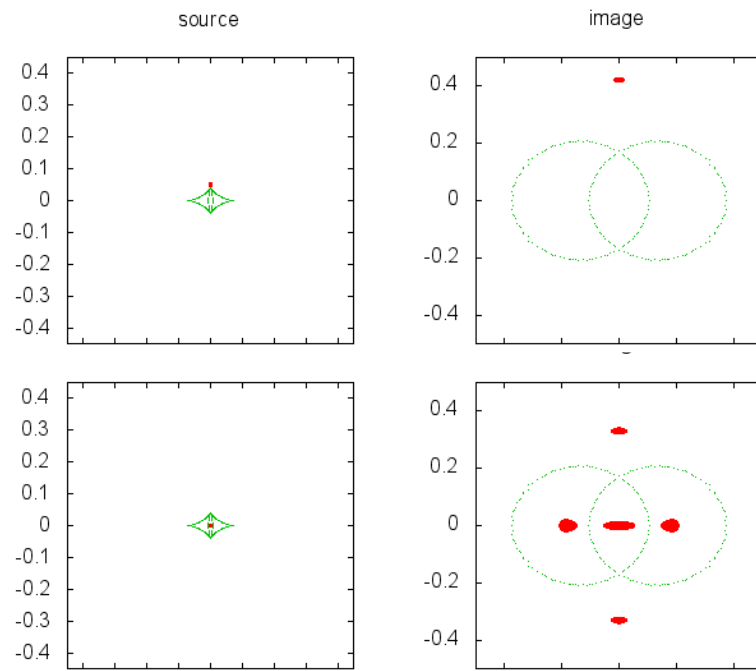
Figure 3.8: Image geometry for two different sources are shown for the critical redshift when the D4 points are formed.
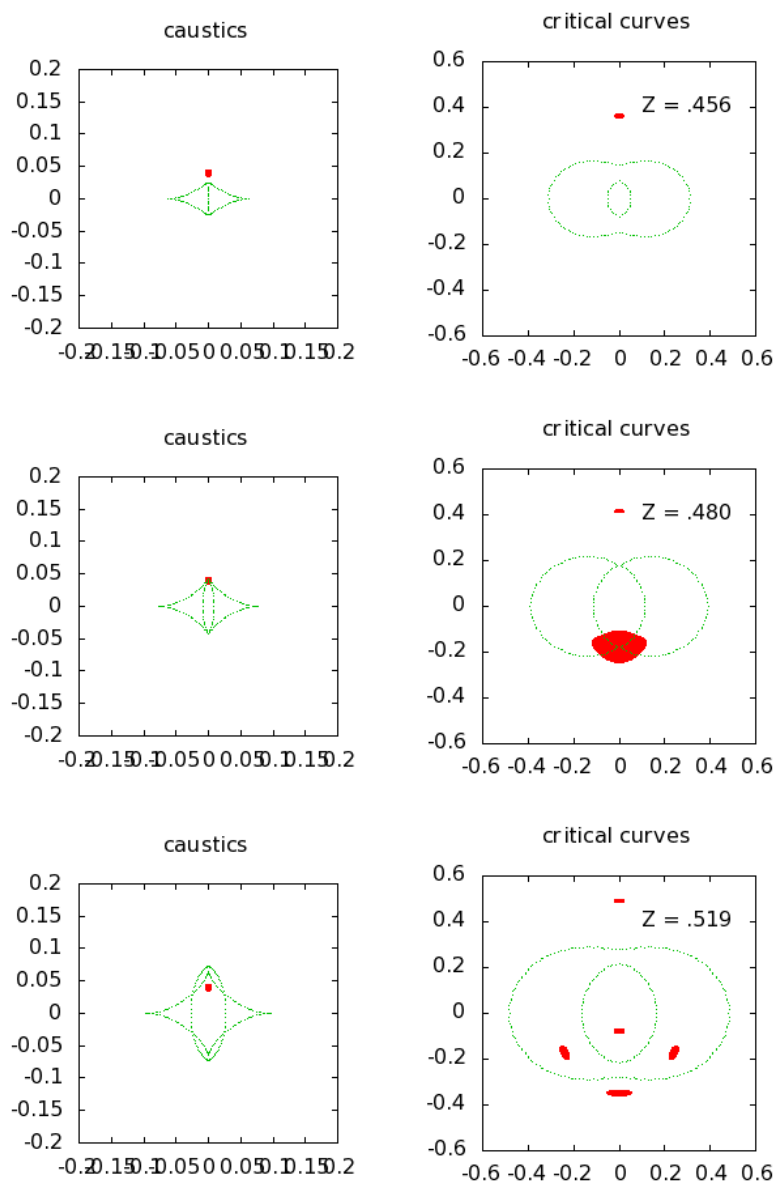
Figure 3.9: Image position for three different redshift values are shown for a fixed source position. D4 points are formed in the central frame. For larger redshifts, five distinct points are formed.
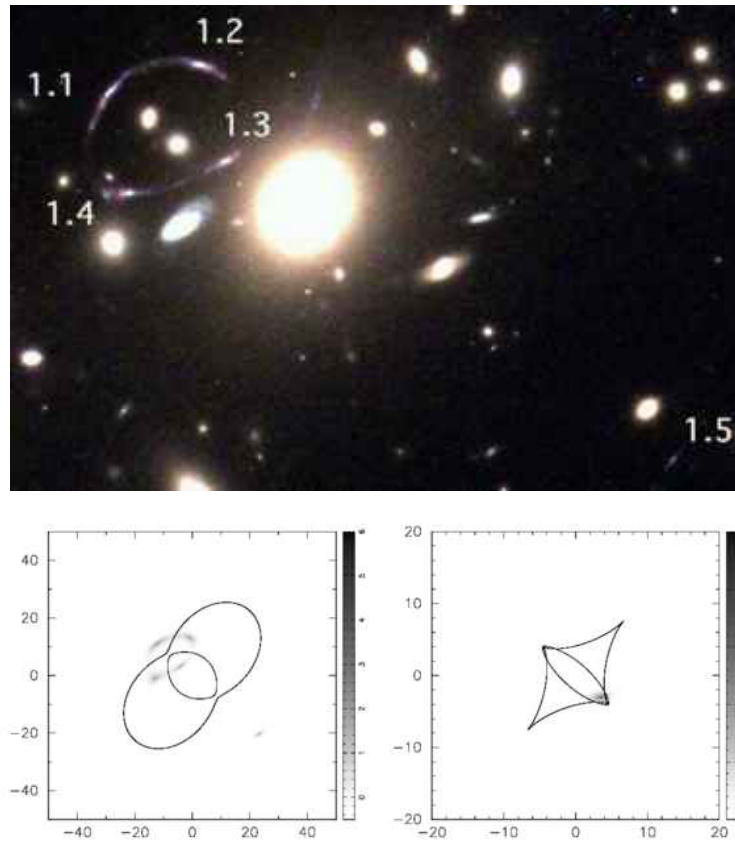
Figure 3.10: Image formation as the source passes through a D4 point reported by Orban de Xivry & Marshall [8] is shown for the Abell 1703 in the top panel. Five images are labelled from 1.1 to 1.5. The corresponding model for the same is shown in the bottom panel (adopted from same references).
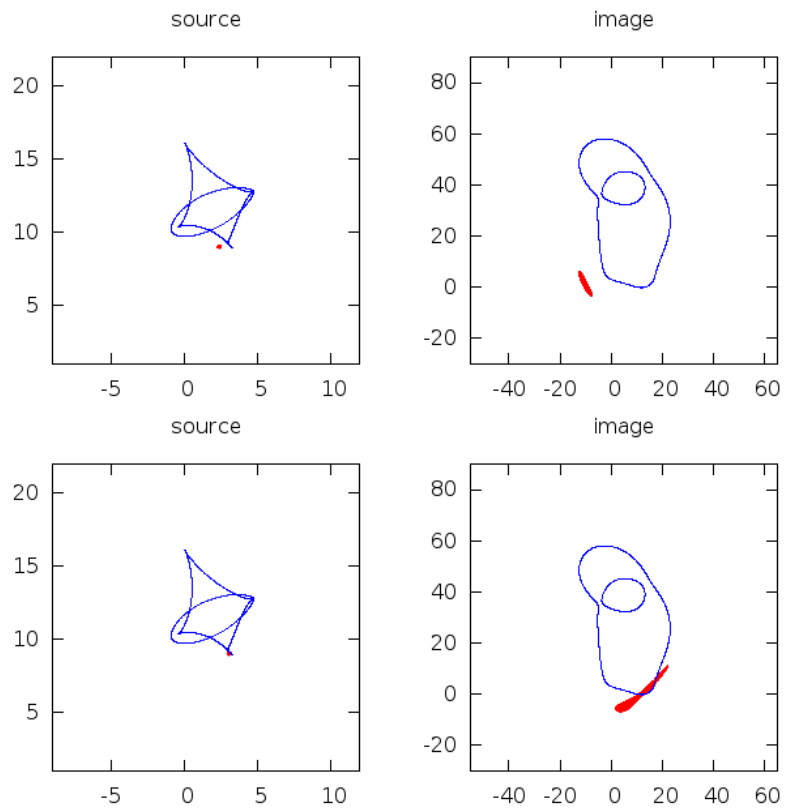
Figure 3.11: Image configurations for different source positions crossing a caustic at A4 point are shown for the two ellipse potential.
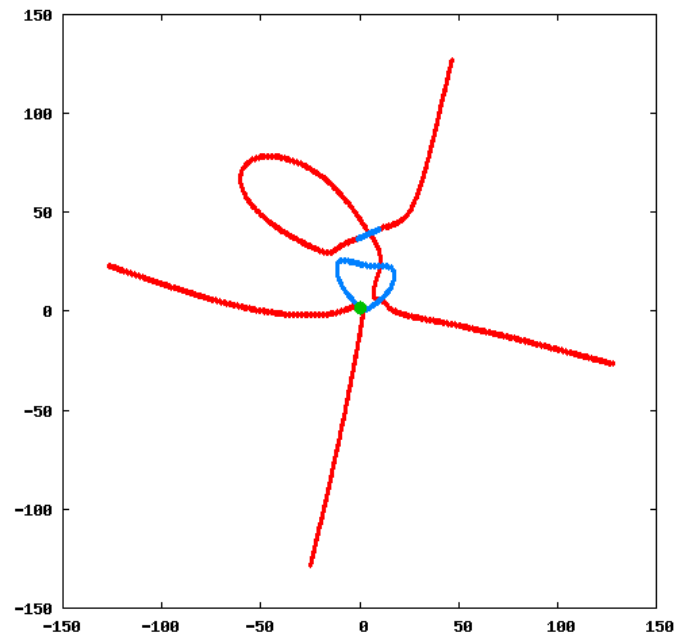
Figure 3.12: Complicated geometry of the A3 lines for two ellipse potential is shown. Two colors (red and blue) gives the A3 lines corresponding to two eigenvalues. A4 point is marked with an green dot in the same plot. Note that the axis labels are arbitrary.
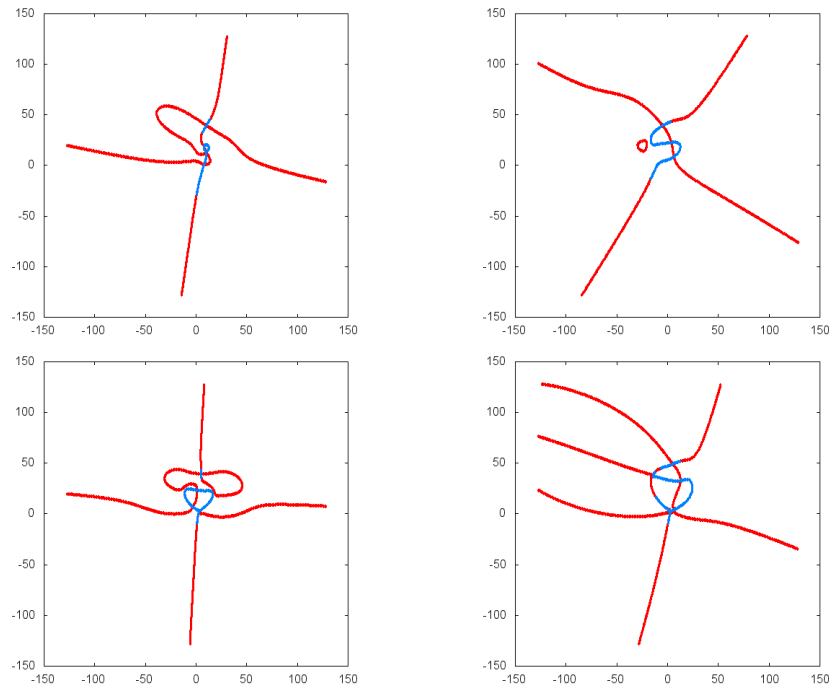
Figure 3.13: Complicated geometry of the A3 lines for two ellipse potential for four different sets of parameters are shown. Two colors (red and blue) gives the A3 lines corresponding to two eigenvalues. In the bottom right figure, four A3 lines of one type merge forming a Pyramid D4 point. Note that the axis labels are arbitrary.
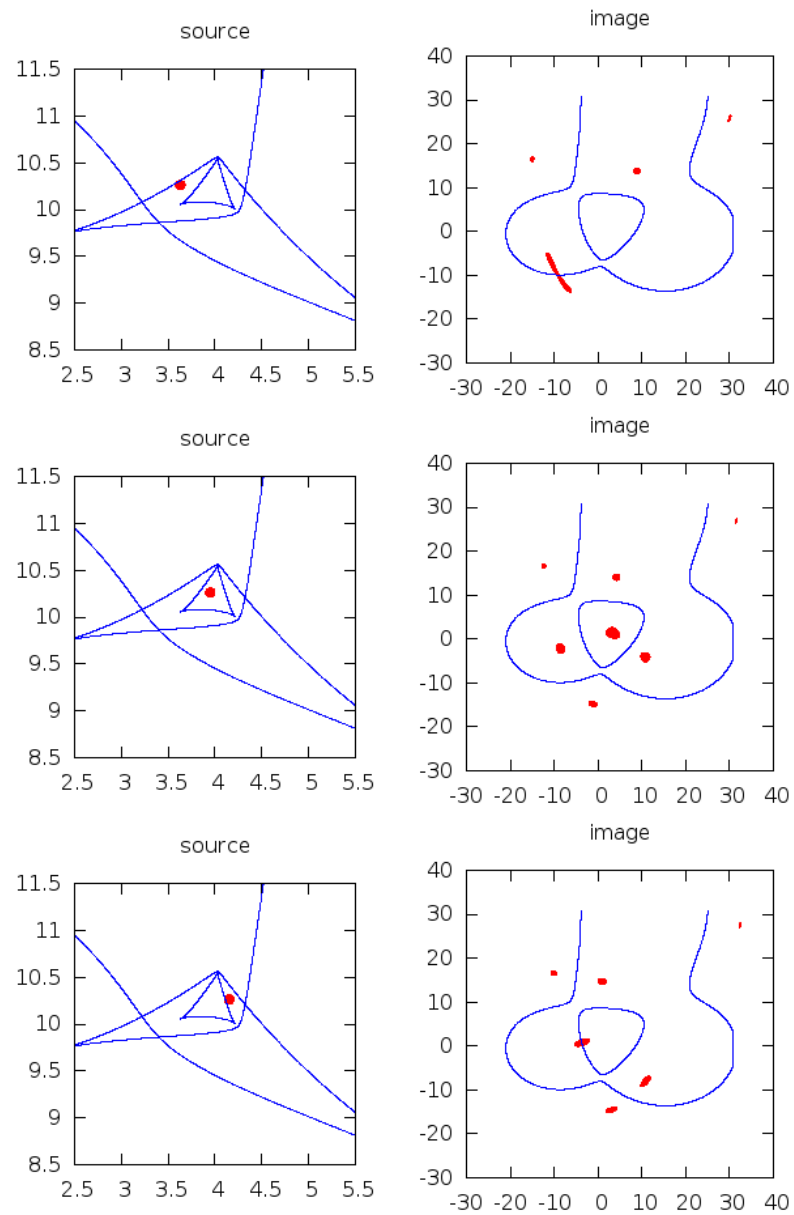
Figure 3.14: Image configurations for different source positions crossing a caustic at Pyramid D4 point are shown for the two ellipse potential. Note that the axis labels are arbitrary.
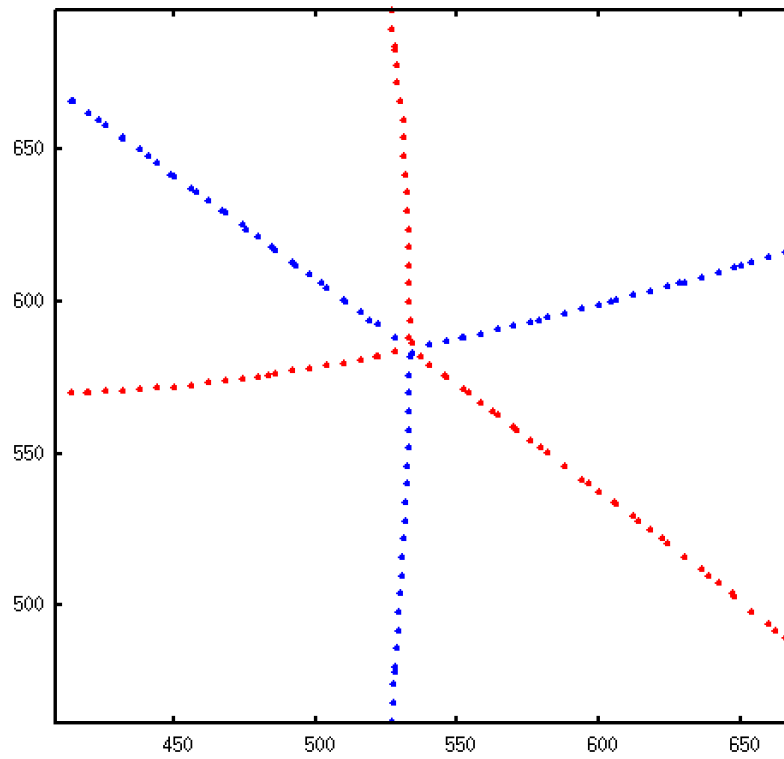
Figure 3.15: A3 lines meeting at the pyramid D4 point. Two colors (red and blue) gives the A3 lines corresponding to two eigenvalues. Note that the axis labels are arbitrary.

Chapter 4

Discussion and Summary

In this project we have analyzed the singularities corresponding to different lensing potentials and image configurations by them for different source positions. Our aim was to examine the formation of different singularities, presumably the higher order singularities, and understand possible image configurations around them. Here we summarize briefly.

- We have developed a software that uses grid based techniques to find the singularities for different lensing potentials. With this, we can give input to an arbitrary lensing potential in a grid and a source gemetry. We have looked at the stable singularities,primarily the cusps and the folds which are formed in a generic lens mapping. We find the A3 lines for all non circularly symmetric lens we have analyzed here. Moving one step ahead, we examined the nature of image formation at certain higher order unstable singularities like the singularities of type D4 and A4.

- Ray shootng method is implemented in our software to find out the image configurations corresponding to different potentials and source positions. Using this we could observe several interesting image formations and plan to construct an atlas of possible image configurations to be observed by future surveys.

- We have considered different simple and complicated lens models influenced by physical scenarios. We discuss in brief our observations with different lens models here. The simplest lens model chosen for our analysis of folds was a circularly symmetric softened isothermal lens. As clear from the simulations, a

source on the positive side of a fold caustic has two images close to and opposite side of the corresponding critical curve. As the source crosses the caustic, the two images move closer together, merge and then disappear. But since such lenses aren't physically realizable we considered the case of lens defined by a elliptical potential. Here we see the cusp caustics which are isolated points connected by folds. A source close to but inside the cusp has three images near the corresponding point on the critical curve. As described for folds, if the source position changes across one of the two curves meeting at cusp, two of the three images merge. When the source crosses the cusp point all the three images merge and a single image remains.

- For a certain sets of lens parameters we investigated the possibility of forming the unstable fixed points of type A4 and D4 given the lens parameters. Here we mainly examined the effect of redshift in a ΛCDM cosmological senario. Although we showed here an example of only one D4 and one A4 point, our software can be used in principle for any arbitrary case.

- Having developed the software, we played with the lens parameters of a double elliptical lens to examine the stable and unstable singularities and image configuration for different cases.
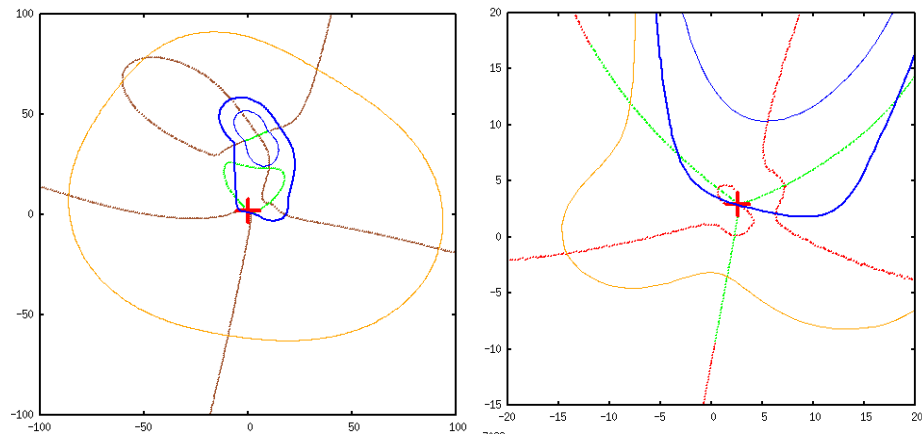

Figure 4.1: A3 lines (green and red) are shown for two potentials giving A4 (left) and pyramid D4 points (right) respectively. Critical curves at three redshifts for the same potentials are also plotted. The A4 and D4 points are marked y a plus sign.

As already mentioned, the goal of this project was to device a methodology that can be used to generate a catalogue of image configurations given different lens potentials. Moreover we are interested in the image configurations near the unstable fixed points, as those allow us to lift some degeneracies of the lensing potentials. Idea is to look for these interesting image configurationss in the upcoming large surveys like LSST and model the lensing potentials. This has already been tried explicitly in Orban de Xivry & Marshall [8], where they have explored different lensing potentials. For each potential, they have considered its evolution over different redshifts of the source and computed the image configurations. This is computationally expensive. We realised, that change in redshift essentially scales the lensing potential keeping its geometrical features intact. This means, the unstable fixed points for any lensing potential can be explored by examining it at any an arbitrary redshift. Figure (4.1) shows the A3 lines formations near the A4 and pyramid D4 points (unstable singularities). Different contours in these figures correspond to the critical curves for the particular lensing potential at different redshifts of the source. These figures clearly demonstrate that though the critical curves changes with redshift of the source, the A3 lines or the A4/D4 points remainthe same. Hence, all we need to do is to check the image configurations near one such A4/D4 point for a particular lensing potential and study the occurrence of these points for different lenses. This will allow us to explore the parameter space of the lens considerably faster than the method suggested before. This is a major understanding of our work.

Future Scope

A major problem in gravitational lensing studies is that the degenaracy in the lens configurations can give rise to similar image configurations. This is mostly because the hitherto observed gravitational lenses are presumably around the stable singularities. Lensing around an unstable singularity is rare as it resuires the right arrangement of the lens parameters to form one, but is most useful becasue of the same reason at the same time. Finding such cases reduces the degenaricies in the lensing parameters drasticaly. In the history of gravitational lensing, though the generic lens singularities have been studied in great detail, not much progress has been made in studying the unstable singularities. An important reason for the latter is the limited number of known lenses. But with the advent of new generation of

telescopes like the Large Synoptic Survey Telescope (LSST) the number of lenses will increase by a factor greater than ten. Such surveys will have an improved sensitivity and the potential to detect these rare images in the sky. As per our study, we plan to perform the following in future.

- Having developed a systematic technique for finding the stable and unstable singularities, it helps us to prepare for the image configurations we expect from the different singularities. We plan to study the parameter space in detail with the present software and investigate the image configurations around the natural cases of the galaxy cluster potentials etc.

- Our gridding technique uses a single resolution grid as present, which has limitation of resolution to the image size. This can be overcome with a adaptive mesh technique, which we shall like to implement.

- In the present version of the implementation, we have only considered the image positions for different lens geometry and source positions, magnification of the image is not considered explicitly. In practice magnification of the image will play a crucial role in modelling different observed image configurations, therefore we aim to implement it in our software in future.

- We also plan to use our models to study the observed data and draw conclusions about the potential of the clusters in consideration.

Bibliography

[1] Arnold, V. I., Shandarin, S. F., & Zeldovich, I. B. 1982, Geophysical and Astrophysical Fluid Dynamics, 20, 111

[2] Cabanac, R. A., Valls-Gabaud, D., Jaunsen, A. O., Lidman, C., & Jerjen, H. 2005, Astronomy and Astrophysics, 436, L21

[3] Dyson, F. W., Eddington, A. S., & Davidson, C. 1920, Royal Society of London Philosophical Transactions Series A, 220, 291

[4] Einstein, A. 1936, Science, 84, 506

[5] Zwicky, F. 1937, Astrophysical Journal, 86, 217

[6] Walsh, D., Carswell, R. F., & Weymann, R. J. 1979, Nature, 279, 381

[7] Narayan, R., & Bartelmann, M. 1996, arXiv:astro-ph/9606001

[8] Orban de Xivry, G., & Marshall, P. 2009, Monthly Notices of Royal Astronomical Society, 399, 2

[9] Schneider, P., Ehlers, J., & Falco, E. E. 1992, Gravitational Lenses, XIV, 560 pp. 112 figs.. Springer-Verlag Berlin Heidelberg New York. Also Astronomy and Astrophysics Library,